International Journal of Mathematical Archive-4(3), 2013, 215-227
Available online through www.ijma.info ISSN 2229 – 5046

FINITE ELEMENT ANALYSIS OF CONVECTIVE HEAT AND MASS TRANSFER FLOW OVER A STRETCHING SHEET EMBEDDED IN A POROUS MEDIUM WITH CHEMICAL REACTION, SORET AND RADIATION ABSORPTION

R. Bhuvana vijaya[1], B. Mallikarjuna[1*] and D. R. V. Prasada Rao[2]

[1]Department of Mathematics, Jawaharlal Nehru Technological University Anantapur, AP, India-515002
[2]Department of Mathematics, Sri Krishnadevaraya University, Anantapur, AP, India-515003

(Received on: 02-02-13; Revised & Accepted on: 01-03-13)

ABSTRACT

We investigate the mathematical model of convective heat and mass transfer flow over a stretching sheet embedded in a porous medium under the influence of chemical reaction, radiation absorption and Soret effect. The governing fundamental equations are first transformed into system ordinary differential equations using self similarity transformation and they are then solved numerically by using Galerkin Finite Element method. Important features of flow, heat and mass transfer characteristic for different values of Schmidt number, Buoyancy ratio, chemical reaction, radiation absorption and Soret effect are analyzed and discussed. Favorable comparisons with previously published work on various special cases of the problem are obtained. Numerical results for velocity, temperature and concentration distributions for a prescribed various parameters as well as Nusselt number and Sherwood number with different parameters are reported graphically.

Key words: *Heat and Mass transfer; stretching sheet; Chemical reaction; Radiation absorption and Soret effect.*

INTRODUCTION

Recently, studies on the boundary layer flow and Heat and mass transfer problems on mixed convection flow due to stretching porous medium have received considerable attention because of numerous applications in geophysics and energy related engineering problems that include both metal and polymer sheets. For example, it occurs in the extrusion of a polymer sheet from a die or in the drawing of plastic films, which are then cooled in a cooling bath and during cooling reduction to both thickness and width takes place. The quality of the final product depends on the rate of heat transfer at the stretching surface and it occurs in the aerodynamic extrusion of polymer sheets, fiber and granular insulation materials, high performance insulation buildings, transpiration cooling, packed bed chemical reactors and continuous filament extrusion from a dye. Sakiadis [1] initiated the study of boundary layer flow over a continuous solid surface moving with a constant speed. Crane [2] gave an exact similarity solution in closed analytical form for steady boundary layer flow of an incompressible viscous fluid caused due to stretching of an elastic sheet which moves in its own plane with a velocity varying linearly with distance from a fixed point.

In many practical applications mass transfer takes place by diffusive operations which involve the molecular diffusion of species in the presence of two types of chemical reactions namely, homogeneous and heterogeneous. Mixed convective heat and mass transfer problems with chemical reaction are of importance in many processes and have, therefore, received a considerable amount of attention in recent years. In processes such as drying, evaporation at the surface of a water body, energy transfer in a wet cooling tower and the flow in a desert cooler, heat and mass transfer occur simultaneously. Possible applications of this type of flow

NOMENCLATURE

u	velocity of the fluid in the x-direction
v	velocity of the fluid in the y-direction
x	flow directional coordinate along the stretching sheet
y	distance normal to the stretching sheet
T	temperature of the fluid
T_m	mean fluid temperature
T_w	stretching sheet temperature
T_∞	temperature far away from the stretching sheet
C	concentration of the species
c_b	drag coefficient which is independent of viscosity

c_p	Specific heat at constant pressure
D_m	mass diffusion coefficient
A_o	parameters of temperature distribution on the stretching surface
A_1	parameter of mass distribution on the stretching surface
A^*,B^*	coefficients of space and temperature dependent heat source/sink
b	stretching parameter
$\vec{B}$	transverse magnetic field
B_o	uniform transverse magnetic field
E	electric field
E_c	Eckert number
E_o	uniform electric field
E_1	local electromagnetic parameter
F^*	local inertia-coefficient
Gr_x	Grashof number
g	acceleration due to gravity
Ha	Hartmann number
k	permeability of the porous medium
k_1	porous parameter
k_T	thermal diffusion ratio
K	mean absorption coefficient
Pr	Prandtl number
Sr	Soret number
Sc	Schmidt number
q'''	non-uniform heat source/sink
Re_x	local Reynolds number
Nu_x	local Nusselt number
Sh_x	local Sherwood number
Greek symbols	
θ	non-dimensional temperature parameter
θ_r	constant, related to variable viscosity
β_T	co-efficient of thermal expansion
η	similarity variable
κ	is the thermal conductivity
ν	kinematic viscosity
ρ	density of the fluid
σ	magnetic permeability
λ	buoyancy parameter or mixed convection parameter

can be found in many industries. For instance, in the power industry, among the methods of generating electric power is one in which electrical energy is extracted from a moving conducting fluid. We are interested in cases in which diffusion and chemical reaction occur at roughly the same speed. When diffusion is much faster than chemical reaction, then only chemical factors influence the chemical reaction rate; when diffusion is not much faster than reaction, the diffusion and kinetics interact to produce very different effects.In view of these applications, [3-8] have studied and reported the significance of chemical reaction. The study of heat generation or absorption effects in moving fluids is important in view of several physical problems, such as fluids undergoing exothermic or endothermic chemical reaction.

The effects of thermal-diffusion (Soret) of heat and mass transfer have been examined by chapman and cowling [9] and Hirshfelder et al., [10] from the kinetic theory of gases. Thedy explained the phenomena and derived the necessary formulae to calculate the thermal-diffusion coefficient and thermal-diffusion factor for monatomic gases or polyatomic gas mixtures. The heat and mass transfer simultaneously affecting each other that will cause the cross-diffusion effect. The mass transfer caused by temperature gradients is called Soret or thermal-diffusion effect. Thus Soret effect is referred to species differentiation developing in an initial homogeneous mixture submitted to a thermal gradient. The Soret effect, for example, has been utilized for isotope separation, and in mixture between gases with very light molecular weight (H_2, H_e) and of medium molecular weight (N_2, air). The previous studies are based on the constant physical parameters of the fluid. For most realistic fluids, the viscosity shows a rather pronounced variation with temperature. It is known that the fluid viscosity changes with temperature. Thus it is necessary to take into account the variation of viscosity with temperature in order to accurately predict the heat transfer rates. Ali [11] investigated the effect of variable viscosity on mixed convection heat transfer along a moving surface. Recently, Mondal et. al., [12] have studied MHD non-Darcy mixed convective diffusion of species over a stretching sheet embedded in a porous medium with non-uniform heat source/sink, variable viscosity and Soret effect.

The effect of the chemical reaction and radiation absorption on the unsteady MHD free convection flow past a semi infinite vertical permeable moving plate with heat source and suction investigate by Ibrahim and Elaiw *et.al.* [13]. Jafarunnisa [14] have studied the effect of radiation absorption on unsteady convective heat and mass transfer flow with chemical reaction. Naga Leela Kumari [15] have discussed effect of radiation absorption on unsteady hydromagnetic convective heat and mass transfer flow in a horizontal channel bounded flat walls with oscillatory flux. Indudara Reddy [16] have studied effect of radiation absorption on unsteady hydro magnetic convective heat and mass transfer flow through a porous medium past a semi infinite vertically porous plate.

The motivation of this analysis is to investigate the effect of radiation absorption on convective heat and mass transfer flow of a chemically reacting viscous electrically conducting fluid with non-uniform heat source past a stretching sheet embedded in a porous medium. The flow characteristics are analyzed for different variations of chemical reaction, radiation absorption and buoyancy ration and Soret effect. The rate of heat and mass transfer are evaluated numerically.

MATHEMATICAL ANALYSIS

Consider two dimensional steady incompressible electrically conducting fluid flow over a vertical non linear stretching sheet embedded in non-Darcy porous medium with the plane y=0 of a co-ordinate system. The fluid properties are assumed to be isotropic and

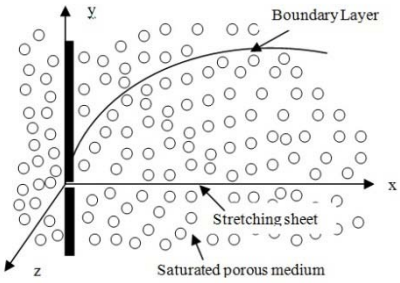

Fig-1: Boundary layer over stretching sheet

constant, except for the fluid viscosity μ which is assumed to vary as be an inverse linear function of temperature T, in the form (see Lai and Kulacki [17]):

$$\frac{1}{\mu} = \frac{1}{\mu_\infty}\left[1+\gamma(T-T_\infty)\right] \quad \text{or} \quad \frac{1}{\mu} = a\,(T-T_r)\,, \tag{1}$$

Where $a = \dfrac{\gamma}{\mu_\infty}$ and $T_r = \left(T_\infty - \dfrac{1}{\gamma}\right)$. Both *a* and T_r are constant and their values depend on the reference state and the thermal property of the fluid, i.e. γ. In general, *a>0* for liquids and *a<0* for gases. θ_r is a constant which is defined by $\theta_r = \dfrac{T_r - T_\infty}{T_w - T_\infty} = -\dfrac{1}{\gamma(T_w - T_\infty)}$ and primes denote differentiation with respect to η. It is worth mentioning here that for $\gamma \to 0$ i.e. $\mu = \mu_\infty$ (constant) then $\theta_r \to \infty$. It is also important to note that θ_r is negative for liquids and positive for gases. T_∞ is free stream temperature. The flow region is exposed under uniform transverse magnetic fields $B_0 = (0, B_0, 0)$ and uniform electric field $\vec{E} = (0,0,-E_0)$ (see Fig.1). Since such imposition of electric and magnetic fields stabilizes the boundary layer flow. It is assumed that the flow is generated by stretching of an elastic boundary sheet from a slit by imposing two equal and opposite forces in such a way that velocity of the boundary sheet is of linear order of the flow direction. We know from Maxwell's equation that $\nabla \cdot \vec{B} = 0$ and $\nabla \times \vec{E} = 0$. When magnetic field is not so strong then electric field and magnetic field obeys Ohm's law $\vec{J} = \sigma(\vec{E} + \vec{q} \times \vec{B})$, where $\vec{J}$ is the Joule current. The viscous dissipation and velocity of the fluid far away from the plate are assumed to be negligible. We assumed that magnetic Reynolds number of the fluid is small so that induced magnetic field and Hall effect may be neglected. We take into account of magnetic field effect as well as electric field in momentum. Under the above stated physical situation, the governing boundary layer equations for momentum and energy for mixed convection under Boussinesq's approximation are

Conservation of mass:

$$\frac{\partial u}{\partial x} + \frac{\partial v}{\partial y} = 0. \tag{2}$$

Conservation of momentum:

$$\frac{1}{\varepsilon^2}\left(u\frac{\partial u}{\partial x}+\frac{\partial u}{\partial y}\right)=\frac{1}{\rho_\infty \varepsilon}\frac{\partial}{\partial y}\left(\mu\frac{\partial u}{\partial y}\right)+\frac{\sigma}{\rho_\infty}\left(E_0B_0-{B_0}^2u\right)-\frac{\upsilon}{k}u-\left(\frac{C_b}{\sqrt{k}}\right)u^2+g\beta_T\left(T-T_\infty\right)+g\beta_C(C-C_\infty) \quad (3)$$

Energy equation:

$$u\frac{\partial T}{\partial x}+v\frac{\partial T}{\partial y}=\frac{k}{\rho_\infty C_p}\frac{\partial^2 T}{\partial y^2}+\frac{\mu}{\rho_\infty C_p}\left(\frac{\partial u}{\partial y}\right)^2+\frac{\sigma}{\rho_\infty C_p}\left(uB_0-E_0\right)^2+\frac{1}{\rho_\infty C_p}q'''+{Q_1}^1\left(C-C_\infty\right) \quad (4)$$

Mass diffusion of species equation:

$$u\frac{\partial C}{\partial x}+v\frac{\partial C}{\partial y}=D_m\frac{\partial^2 C}{\partial y^2}+\frac{D_m k_T}{T_m}\frac{\partial^2 T}{\partial y^2}-\gamma^1\left(C-C_\infty\right) \quad (5)$$

Boundary conditions

$$\begin{aligned} &u=U_w(x)=bx,\quad v=0,\quad T=T_w=T_\infty+A_0\left(\frac{x}{l}\right)^2\\ &C=C_w=C_\infty+A_1\left(\frac{x}{l}\right)^2 \quad at\ \ y=0\\ &u=0,\quad T\to T_\infty,\quad C\to C_\infty,\qquad as\ \ y\to\infty \end{aligned} \quad (6)$$

where u and v are the velocity components in the x and y-directions respectively: C_w stands for concentration at wall, C_∞ is the concentration far away from the stretching sheet, D_m is the mass diffusivity, T_m is the mean fluid temperature, k_T is the thermal diffusion ratio, ${Q_1}^1$ is the radiation absorption coefficient and γ^1 is the chemical reaction coefficient. To solve the governing boundary layer equations (2)-(5), the following similarity transformations are introduced (see [18, 19]):

$$\begin{aligned} &u=bxf'(\eta),\quad v=-\sqrt{b\upsilon_\infty}\,f(\eta),\quad \eta=\sqrt{\frac{b}{\upsilon_\infty}}y.\\ &\theta=\frac{T-T_\infty}{T_w-T_\infty},\quad \phi(\eta)=\frac{C-C_\infty}{C_w-C_\infty}. \end{aligned} \quad (7)$$

The non-uniform heat source/sink, q''' (see [20,21]) is modeled as

$$q'''=\frac{ku_w(x)}{x\upsilon_\infty}\left[A^*\left(T_w-T_\infty\right)e^{-\eta}+\left(T-T_\infty\right)B^*\right], \quad (8)$$

where A^* and B^* are the coefficient of space and temperature dependent heat source/sink respectively. Here we make a note that the case $A^*>0$, $B^*>0$ corresponds to internal heat generation and that $A^*<0$, $B^*<0$ corresponds to internal heat absorption.

Substitution of equation (7) and (8) into the governing equations (3)-(5) and using the above relations we finally obtain a system of non-linear ordinary differential equations with appropriate boundary conditions

$$\frac{f'''}{\varepsilon}+\left(1-\frac{\theta}{\theta_r}\right)\frac{ff''}{\varepsilon^2}+\frac{1}{\theta_r-\theta}\frac{\theta' f''}{\varepsilon}+\left(1-\frac{\theta}{\theta_r}\right)M^2\left(E_1-f'\right)=\left(1-\frac{\theta}{\theta_r}\right)\left(\frac{f'^2}{\varepsilon^2}+F^*f'^2-\lambda\left(\theta+N\varphi\right)\right)+k_1f' \quad (9)$$

$$\theta''-\left(1-\frac{\theta}{\theta_r}\right)\Pr\left[\left(2f'\theta-f\theta'\right)-M^2Ec\left(E_1-f'\right)^2\right]=-Ec\Pr\left(f''\right)^2-\left(A^*e^{-\eta}+B^*\theta\right)-Q_1\phi \quad (10)$$

$$\phi''+Sc\left(f\phi'-2f'\phi\right)-\gamma\phi=-ScSr\theta'' \quad (11)$$

The boundary condition (6) becomes

$$f(0)=0,\quad f'(0)=1,\quad \theta(0)=1,\quad \phi(0)=1 \text{ at } \eta\to 0,$$
$$f'(\infty)=0,\quad \theta(\infty)=0,\quad \phi(\infty)=0 \text{ as } \eta\to\infty, \tag{12}$$

where $k_1=\frac{\upsilon_\infty}{kb}$ is the porous parameter, $M=\sqrt{\frac{\sigma}{\rho b}}B_0$ is the Hartmann number, $E_1=\frac{E_0}{B_0 bx}$ is the local inertial-coefficient, $\lambda=\frac{g\beta_T(T_w-T_\infty)}{b^2x}$ is the buoyancy or mixed convection parameter, $\Pr=\left(1-\frac{\theta}{\theta_r}\right)^{-1}\Pr_\infty$ is the Prandtl number and $\Pr_\infty=\frac{\rho_\infty\upsilon_\infty C_p}{k}$ is the ambient Prandtl number, and $Ec=\frac{b^2l^2}{A_0C_p}$ is the Eckert number, $Sc=\frac{\upsilon_\infty}{D_m}$ is the Schmidt number.

The local Nusselt number which are defined as

$$Nu_x=\frac{xq_w}{k(T_w-T_\infty)}, \tag{13}$$

where q_w is the heat transfer from the sheet is given by

$$q_w=-k\left(\frac{\partial T}{\partial y}\right)_{y=0}, \tag{14}$$

Using the non-dimensional variables (7), we get from equations (13) and (14) as

$$\frac{Nu_x}{\mathrm{Re}_x^{1/2}}=-\theta'(0). \tag{15}$$

The physical quantity of interest is the local Sherwood number which are defined as

$$Sh_x=\frac{xq_m}{D_m(C_w-C_\infty)}, \tag{16}$$

Where q_m is the mass transfer which is defined by

$$q_m=-D_m\left(\frac{\partial C}{\partial y}\right)_{y=0} \tag{17}$$

Using the non-dimensional variables (7) and (17), we get from equation (16) as

$$\frac{Sh_x}{\mathrm{Re}_x^{1/2}}=-\phi'(0),$$

where $\mathrm{Re}_x=\frac{xU_w(x)}{\upsilon_\infty}$ is the local Reynolds number.

Finite Element Analysis

The set of differential equations given in (9)-(11) are highly non-linear and therefore, cannot be solve analytically. Hence finite element method has been used for solving it. The finite element method is powerful technique for solving ordinary and partial differential equations. This method is so general that it can be applied to a wide variety of engineering problems including heat and mass transfer, fluid mechanics and solid mechanics, electrical systems, chemical processing. For the finite element method one can refers to Bathe [22] and Reddy [23].

We define the error residuals as

$$E_f^k = \frac{1}{\varepsilon}\frac{d}{d\eta}\frac{d^2 f^k}{d\eta^2} + \left(1-\frac{\theta^k}{\theta_r}\right)\frac{f^k}{\varepsilon^2}\frac{d^2 f^k}{d\eta^2} + \frac{1}{\theta_r-\theta^k}\frac{d}{d\eta}\left(\theta^k\frac{df^k}{d\eta}\right) + \left(1-\frac{\theta^k}{\theta_r}\right)M^2\left(E_1-\frac{df^k}{d\eta}\right) - \left(1-\frac{\theta^k}{\theta_r}\right)\left(\left(\frac{df^k}{d\eta}\right)^2\left(F^*+\frac{1}{\varepsilon^2}\right)-\lambda\left(\theta^k+N\phi^k\right)\right) - k_1\frac{df^k}{d\eta} \quad (18)$$

$$E_\theta^k = \frac{d}{d\eta}\frac{d\theta^k}{d\eta} - \left(1-\frac{\theta^k}{\theta_r}\right)\Pr\left[\left(2\theta^k\frac{df^k}{d\eta} - f^k\frac{d\theta^k}{d\eta}\right) - M^2 Ec\left(E_1-\frac{df^k}{d\eta}\right)^2\right] + Ec\,\Pr\left(\frac{d^2 f^k}{d\eta^2}\right)^2 + \left(A^* e^{-\eta} + B^*\theta^k\right) + Q_1\phi^k \quad (19)$$

$$E_\phi^k = \frac{d}{d\eta}\frac{d\phi^k}{d\eta} + Sc\left(f^k\frac{d\phi^k}{d\eta} - 2\frac{df^k}{d\eta}\phi^k\right) - \gamma\phi^k + ScSr\frac{d}{d\eta}\frac{d\theta^k}{d\eta} \quad (20)$$

where f^k, θ^k & ϕ^k are the values of f, θ & φ in the arbitrary element e_k.

Variational formulation

The variational form associated with equations (18)-(20) over a typical element (η_e, η_{e+1}) is given by

$$\int_{\eta_e}^{\eta_e+1} w_1 E_f^k d\eta = 0 \quad (21)$$

$$\int_{\eta_e}^{\eta_e+1} w_2 E_\theta^k d\eta = 0 \quad (22)$$

$$\int_{\eta_e}^{\eta_e+1} w_3 E_\phi^k d\eta = 0 \quad (23)$$

where w_1, w_2 & w_3 are arbitrary test functions and $w_1 = w_2 = w_3 = \Psi_j^k$, $j = 1\,to\,3$.

Finite Element Formulation

The finite element approximations of f^k, θ^k & ϕ^k are taken as,

$$\begin{aligned} f^k &= f_1^k\Psi_1^k + f_2^k\Psi_2^k + f_3^k\Psi_3^k \\ \theta^k &= \theta_1^k\Psi_1^k + \theta_2^k\Psi_2^k + \theta_3^k\Psi_3^k \\ \phi^k &= \phi_1^k\Psi_1^k + \phi_2^k\Psi_2^k + \phi_3^k\Psi_3^k \end{aligned} \quad (24)$$

For a typical element, the interpolation functions (Shaped functions) are given by

$$\Psi_1^k = \frac{\left(\eta-\frac{2k-1}{n}s\right)\left(\eta-\frac{2k}{n}s\right)}{s\left(\frac{2k-2}{n}-\frac{2k-1}{n}\right)s\left(\frac{2k-2}{n}-\frac{2k}{n}\right)}$$

$$\Psi_2^k = \frac{\left(\eta-\frac{2k-2}{n}s\right)\left(\eta-\frac{2k}{n}s\right)}{s\left(\frac{2k-1}{n}-\frac{2k-2}{n}\right)s\left(\frac{2k-1}{n}-\frac{2k}{n}\right)}$$

$$\Psi_3^k = \frac{\left(\eta-\frac{2k-1}{n}s\right)\left(\eta-\frac{2k-2}{n}s\right)}{s\left(\frac{2k}{n}-\frac{2k-2}{n}\right)s\left(\frac{2k}{n}-\frac{2k-1}{n}\right)}$$

where Ψ_1^k, Ψ_2^k & Ψ_3^k are Lagrange's quadratic polynomials, $k=\frac{n}{2}$ & $s=6$. Following the Galerkin weighted residual method and integrating (18)-(20), we obtain

$$\int_{\eta_e}^{\eta_{e+1}}\frac{1}{\varepsilon}\frac{d^2f^k}{d\eta^2}\frac{d\psi_j^k}{d\eta}d\eta+\int_{\eta_e}^{\eta_{e+1}}\left(1-\frac{\theta^k}{\theta_r}\right)\frac{f^k}{\varepsilon^2}\frac{d^2f^k}{d\eta^2}\psi_j^k d\eta+\int_{\eta_e}^{\eta_{e+1}}\frac{1}{\theta_r-\theta^k}\frac{d}{d\eta}\left(\theta^k\frac{df^k}{d\eta}\right)\psi_j^k d\eta$$
$$+\int_{\eta_e}^{\eta_{e+1}}\left(1-\frac{\theta^k}{\theta_r}\right)M^2\left(E_1-\frac{df^k}{d\eta}\right)\psi_j^k d\eta-\int_{\eta_e}^{\eta_{e+1}}\left(1-\frac{\theta^k}{\theta_r}\right)\left(\left(\frac{df^k}{d\eta}\right)^2\left(F^*+\frac{1}{\varepsilon^2}\right)-\lambda\left(\theta^k+N\phi^k\right)\right)\psi_j^k d\eta$$
$$-\int_{\eta_e}^{\eta_{e+1}}k_1\frac{df^k}{d\eta}\psi_j^k d\eta=P_{2j}+P_{1j} \qquad (25)$$

where $P_{2j}=\left(\frac{df^k}{d\eta}\psi_j^k\right)_{\eta_{e+1}}$ & $P_{1j}=-\left(\frac{df^k}{d\eta}\psi_j^k\right)_{\eta_e}$

$$\int_{\eta_e}^{\eta_{e+1}}\frac{d\theta^k}{d\eta}\frac{d\psi_j^k}{d\eta}d\eta-\int_{\eta_e}^{\eta_{e+1}}\left(1-\frac{\theta^k}{\theta_r}\right)\Pr\left[\left(2\theta^k\frac{df^k}{d\eta}-f^k\frac{d\theta^k}{d\eta}\right)-M^2Ec\left(E_1-\frac{df^k}{d\eta}\right)^2\right]\psi_j^k d\eta$$
$$+\int_{\eta_e}^{\eta_{e+1}}Ec\Pr\left(\frac{d^2f^k}{d\eta^2}\right)^2\psi_j^k d\eta+\int_{\eta_e}^{\eta_{e+1}}\left(A^*e^{-\eta}+B^*\theta^k\right)\psi_j^k d\eta+\int_{\eta_e}^{\eta_{e+1}}Q_1\phi^k\psi_j^k d\eta=Q_{2j}+Q_{1j} \qquad (26)$$

where $Q_{2j}=\left(\frac{d\theta^k}{d\eta}\psi_j^k\right)_{\eta_{e+1}}$ & $Q_{1j}=-\left(\frac{d\theta^k}{d\eta}\psi_j^k\right)_{\eta_e}$

$$\int_{\eta_e}^{\eta_{e+1}}\frac{d\varphi^k}{d\eta}\frac{d\psi_j^k}{d\eta}d\eta+\int_{\eta_e}^{\eta_{e+1}}Sc\left(f^k\frac{d\varphi^k}{d\eta}-2\frac{df^k}{d\eta}\varphi^k\right)\psi_j^k d\eta-\int_{\eta_e}^{\eta_{e+1}}\gamma\varphi^k\psi_j^k d\eta+ScSr\int_{\eta_e}^{\eta_{e+1}}\frac{d\theta^k}{d\eta}\frac{d\psi_j^k}{d\eta}d\eta=S_{2j}+S_{1j} \qquad (27)$$

where $S_{2j}=\left(\frac{d\phi^k}{d\eta}\psi_j^k\right)_{\eta_{e+1}}+\left(\frac{d\theta^k}{d\eta}\psi_j^k\right)_{\eta_{e+1}}$ & $S_{1j}=\left(\frac{d\phi^k}{d\eta}\psi_j^k\right)_{\eta_e}+\left(\frac{d\theta^k}{d\eta}\psi_j^k\right)_{\eta_e}$.

Substituting f^k, θ^k & ϕ^k in terms of local nodal values, the above equations (25)-(27) reduces to

$$\sum_{i=1}^{3}f_i^k\int_{\eta_e}^{\eta_{e+1}}\frac{1}{\varepsilon}\frac{d^2\psi_i^k}{d\eta^2}\frac{d\psi_j^k}{d\eta}d\eta+\sum_{i=1}^{3}f_i^k\int_{\eta_e}^{\eta_{e+1}}\left(1-\frac{\theta^k}{\theta_r}\right)\frac{\psi_i^k}{\varepsilon^2}\frac{d^2\psi_i^k}{d\eta^2}\psi_j^k d\eta+\sum_{i=1}^{3}f_i^k\int_{\eta_e}^{\eta_{e+1}}\frac{1}{\theta_r-\theta^k}\frac{d}{d\eta}\left(\theta^k\frac{d\psi_i^k}{d\eta}\right)\psi_j^k d\eta$$
$$+\sum_{i=1}^{3}f_i^k\int_{\eta_e}^{\eta_{e+1}}\left(1-\frac{\theta_i^k}{\theta_r}\right)M^2\left(E_1-\frac{d\psi_i^k}{d\eta}\right)\psi_j^k d\eta-\sum_{i=1}^{3}f_i^k\int_{\eta_e}^{\eta_{e+1}}\left(1-\frac{\theta^k}{\theta_r}\right)\left(\left(\frac{d\psi_i^k}{d\eta}\right)^2\left(F^*+\frac{1}{\varepsilon^2}\right)-\lambda\left(\theta^k+N\phi^k\right)\right)\psi_j^k d\eta$$
$$-\sum_{i=1}^{3}f_i^k\int_{\eta_e}^{\eta_{e+1}}k_1\frac{d\psi_i^k}{d\eta}\psi_j^k d\eta=P_{2j}+P_{1j} \qquad (28)$$

$$\sum_{i=1}^{3}\theta_i^k\int_{\eta_e}^{\eta_{e+1}}\frac{d\psi_i^k}{d\eta}\frac{d\psi_j^k}{d\eta}d\eta-\sum_{i=1}^{3}\theta_i^k\int_{\eta_e}^{\eta_{e+1}}\left(1-\frac{\psi_i^k}{\theta_r}\right)\Pr\left[\left(2\psi_i^k\frac{df^k}{d\eta}-f^k\frac{d\psi_i^k}{d\eta}\right)-M^2Ec\left(E_1-\frac{df^k}{d\eta}\right)^2\right]\psi_j^k d\eta$$
$$+\sum_{i=1}^{3}\theta_i^k\int_{\eta_e}^{\eta_{e+1}}Ec\Pr\left(\frac{d^2\psi_i^k}{d\eta^2}\right)^2\psi_j^k d\eta+\sum_{i=1}^{3}\theta_i^k\int_{\eta_e}^{\eta_{e+1}}\left(A^*e^{-\eta}+B^*\psi_i^k\right)\psi_j^k d\eta+\sum_{i=1}^{3}\theta_i^k\int_{\eta_e}^{\eta_{e+1}}Q_1\phi^k\psi_j^k d\eta=Q_{2j}+Q_{1j} \qquad (29)$$

Corresponding author: B. Mallikarjuna[1*]
[1]*Department of Mathematics, Jawaharlal Nehru Technological University Anantapur, AP, India-515002*

$$\sum_{i=1}^{3}\phi_i^k\int_{\eta_e}^{\eta_{e+1}}\frac{d\psi_i^k}{d\eta}\frac{d\psi_j^k}{d\eta}d\eta+\sum_{i=1}^{3}\phi_i^k\int_{\eta_e}^{\eta_{e+1}}Sc\left(f^k\frac{d\psi_i^k}{d\eta}-2\frac{df^k}{d\eta}\psi_i^k\right)\psi_j^k d\eta-\sum_{i=1}^{3}\phi_i^k\int_{\eta_e}^{\eta_{e+1}}\gamma\psi_i^k\psi_j^k d\eta$$

$$+ScSr\sum_{i=1}^{3}\phi_i^k\int_{\eta_e}^{\eta_{e+1}}\frac{d\theta^k}{d\eta}\frac{d\psi_j^k}{d\eta}d\eta=S_{2j}+S_{1j} \tag{30}$$

Choosing ψ_j^k's corresponding to each element e_k in the equations (28)-(30) yields a local stiffness matrix of order 3×3 in the form

$$\left(a_{ij}^k\right)\left(f_i^k\right)+\left(b_{ij}^k\right)\left(f_i^k\right)+\left(c_{ij}^k\right)\left(f_i^k\right)+M^2\left(d_{ij}^k\right)\left(f_i^k\right)-\left(e_{ij}^k\right)\left(f_i^k\right)-k_1\left(F_{ij}^k\right)\left(f_i^k\right)=P_{2j}^k+P_{1j}^k+\left(v_j^k\right) \tag{31}$$

$$\left(\left(g_{ij}^k\right)-\Pr\left(h_{ij}^k\right)+Ec\Pr\left(I_{ij}^k\right)+\left(J_{ij}^k\right)+Q_1\left(K_{ij}^k\right)\right)\left(\theta_i^k\right)=Q_{2j}^k+Q_{1j}^k+\left(v_j^k\right) \tag{32}$$

$$\left(\left(l_{ij}^k\right)+Sc\left(m_{ij}^k\right)-\gamma\left(n_{ij}^k\right)+ScSr\left(o_{ij}^k\right)\right)\left(\phi_i^k\right)=S_{2j}^k+S_{1j}^k+\left(v_j^k\right) \tag{33}$$

where $\left(a_{ij}^k\right),\left(b_{ij}^k\right),\left(c_{ij}^k\right),\left(d_{ij}^k\right),\left(e_{ij}^k\right),\left(F_{ij}^k\right),\left(g_{ij}^k\right),\left(h_{ij}^k\right),\left(I_{ij}^k\right),\left(J_{ij}^k\right),\left(K_{ij}^k\right),\left(l_{ij}^k\right),\left(m_{ij}^k\right),\left(n_{ij}^k\right),\left(o_{ij}^k\right)$ are 3×3 matrices and $v_j^k=-A\int_{\eta_e}^{\eta_{e+1}}\psi_i^k\psi_i^k d\eta$ and $\left(P_{2j}^k\right),\left(P_{1j}^k\right),\left(Q_{2j}^k\right),\left(Q_{1j}^k\right),\left(S_{2j}^k\right),\left(S_{1j}^k\right)$ are 3×1 column matrices and such stiffness matrices (31)-(33) in terms of local nodes in each element are assembled using inter element continuity and equilibrium conditions to obtain the coupled global matrices in terms of the global nodal values of $f,\theta\ \&\ \phi$. The whole domain is divided into a set of 100 line elements equations we obtain a matrix of order 201×201. This system of equations as obtained after assembly of the elements equations is non-linear therefore an iterative scheme has been used to solve it. The system is linearized by incorporating known functions. After applying the given boundary conditions only a system of 195 equations remains for the solution which has been solved using Gauss elimination method. Convergence is assumed when the ratio of every one of $f^k,\theta^k\ \&\ \phi^k$ for last 2 approximations differed from unity by less than 10^{-6} at all values of η in $0<\eta<\eta_\infty$.

Table 1

Comparison of Local Nusselt number $-\theta'(0)$ for Ha=0, $\lambda=0$, Q_1=0, $\gamma=0$ and various values of Pr with Ishak[25], Abel[27] and D.Pal[24].

Pr	Ishak[25]	Abel[27]		D.Pal[24]	Present result
1.0	1.3333	1.3333		1.333333	1.332842
3.0	2.50972	2.50972	2.509725	2.509695	
10	4.7969	4.7969		4.796873	4.801825

Table 2

Comparison of Local Nusselt Number $-\theta'(0)$ for various values of Ec, Pr, A, B with Abel and D.Pal in absence of Hartmann number, porous parameter, chemical reaction and Radiation absorption.

Ec	Pr	A	B	Abel[27]	D.Pal[24]	Present result
0.02	4.0	0.3	0.3	2.68986	2.694002	2.700025

RESULTS & DISCUSSION

In this analysis we analyze the effect of chemical reaction, radiation absorption on non Darcy convective heat and mass transfer flow of viscous electrically conducting fluid over a stretching sheet in the presence of magnetic field. The results are presented graphically in figures (2)-(21) for different parametric variations. Comparisons of the present results with previously works are performed and excellent agreements have been obtained. The non-linear coupled differential equations are solved by Galerkin Finite Element analysis with 3 noded line segments. In the absence of chemical reaction and radiation absorption the results are compared with Dulal pal [24].

The variation of the actual velocity (u) is presented in figures (2)-(6) for different values of Schmidt number Sc, Buoyancy ratio N, Chemical reaction parameter γ, Radiation absorption parameter Q_1 and Soret parameter Sr. Fig-(2) represents the variation of u with Sc. The analysis of the graph reveals that the effect of increasing the value of Sc is to

decrease the velocity distribution in the flow region. Physically, the increase of Sc means the decrease of the molecular diffusivity D, which results in decrease of the momentum boundary layer. Hence velocity of the species is large for smaller values of Sc and lesser for higher values of Sc. Fig-(3) represents u with buoyancy ratio N. It is found that when the molecular buoyancy force dominates over the thermal buoyancy force the actual velocity enhances when the buoyancy forces act in the same direction and for the forces acting in opposite direction u depreciates in the flow region. Fig-(4) represents u with chemical reaction parameter γ. It is found that the velocity experiences an enhancement in the degenerating chemical reaction case and depreciates in the generating chemical reaction case. Fig-(5) represents u with radiation absorption parameter Q_1. We notice that an increase in Q_1 enhances u in the flow region. The effect of thermo diffusion (Soret effect) on u is shown in fig-(6). It is found that an increase in the Soret parameter Sr results in a depreciation in the actual velocity.

The non-dimensional temperature (θ) is shown in figures (7)-(11) for different variation of Sc, N, γ, Q_1 and Sr. It is found that the temperature rises from its prescribed value 1 on the wall η=0 reaches the maximum at η =1.5 and then falls to the prescribed value 0 far away from the boundary. Fig-(7) represents θ with Schmidt number Sc. It is found that lesser the molecular diffusivity smaller the actual temperature in the flow region. Fig-(8) represents θ with buoyancy ratio N. It is observed that when the molecular buoyancy force dominates over the thermal buoyancy force the temperature experiences a depreciation when the buoyancy forces act in the same direction and for the forces acting in opposite directions the temperature enhances in the flow region. Fig-(9) represents θ with chemical reaction parameter γ. It is found that temperature enhances in the degenerating chemical reaction case and depreciates in the generating chemical reaction case. Fig-(10) represents θ with radiation absorption parameter Q_1. It is seen from this figure that the temperature distribution increases with increase in radiation absorption parameter Q_1, more effectively near the surface of the stretching sheet with formation of the peak for higher values of $Q_1 > 2.0$. Fig-(11) represents θ with Soret parameter Sr. It is seen from this figure that the temperature distribution increases with increase in Sr more effectively near the surface of the stretching sheet with formation of the peak at η =1.5 for any Sr far away from the boundary and the temperature depreciates in the flow region.

The non-dimensional concentration C is shown in figures (12)-(16) for different values of Sc, N, γ, Q_1 and Sr. The concentration gradually depreciates from its prescribed value 1 on η=0 and attains the prescribed value 0 far away from the boundary. Fig-(12) represents concentration with Schmidt number Sc. It is notice from the analysis of the graph that an

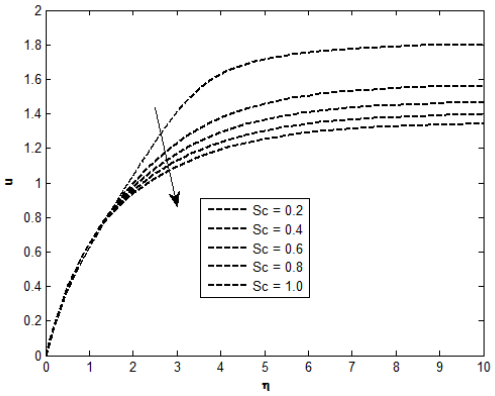

Fig-2: Velocity profile for different values of Sc

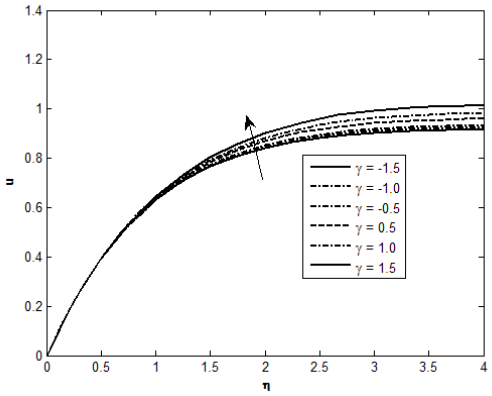

Fig-4: Velocity profile for different values of γ

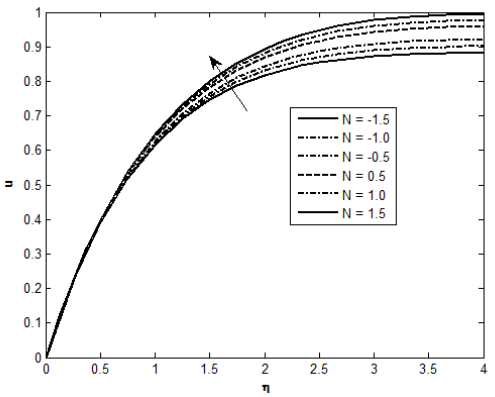

Fig-3: Velocity profile for different values of N

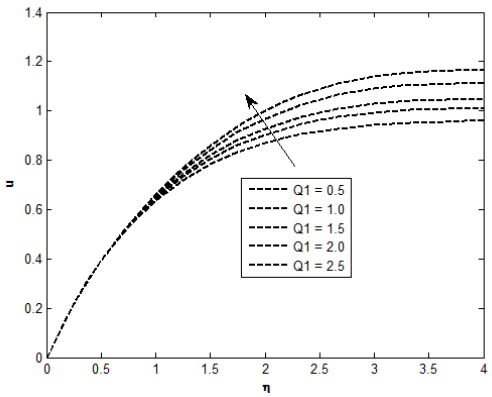

Fig-5: Velocity profile for different values of Q_1

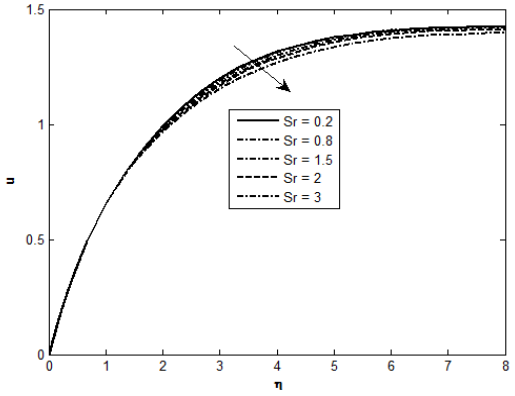

Fig-6: Velocity profile for different values of Sr

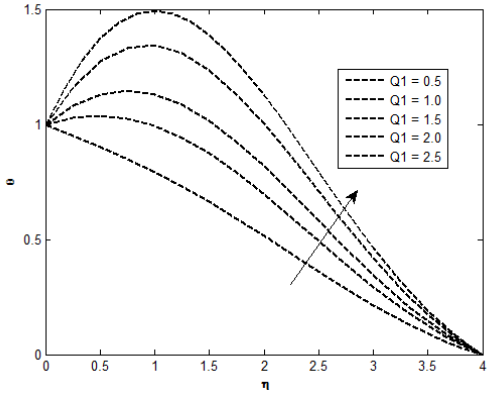

Fig-10: Temperature profile for different values of Q_1

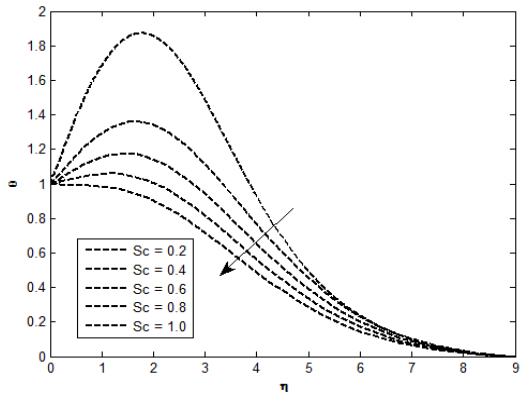

Fig-7: Temperature profile for different values of Sc

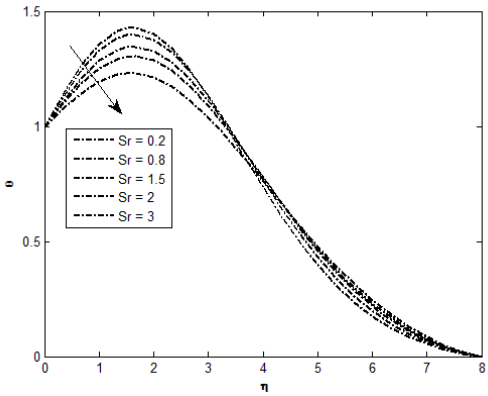

Fig-11: Temperature profile for different values of Sr

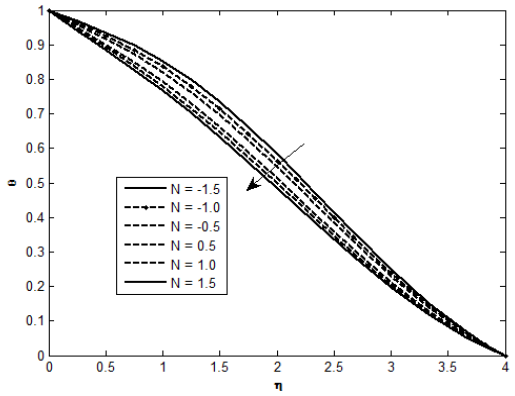

Fig-8: Temperature profile for different values of N

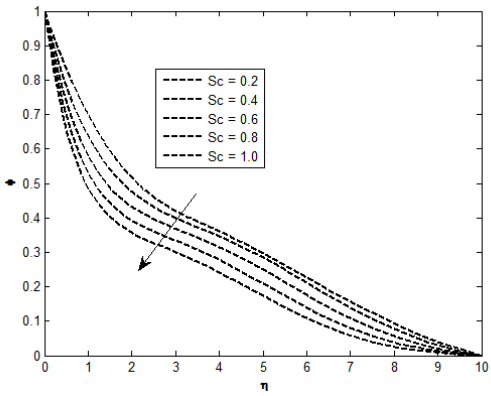

Fig12: Concentration profile for different values of Sc

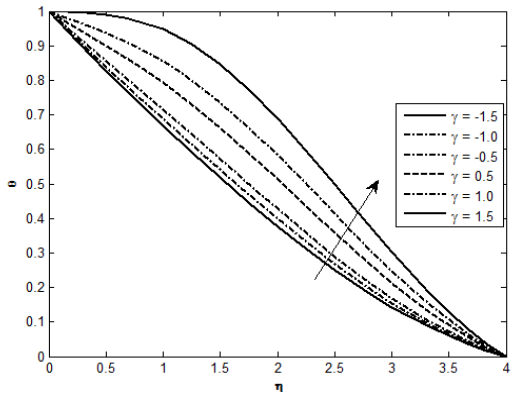

Fig-9: Temperature profile for different values of γ

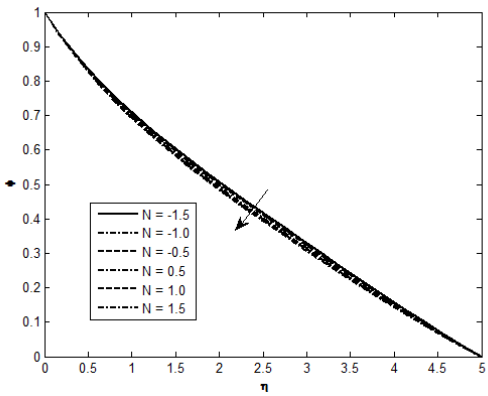

Fig13: Concentration profile for different values of N

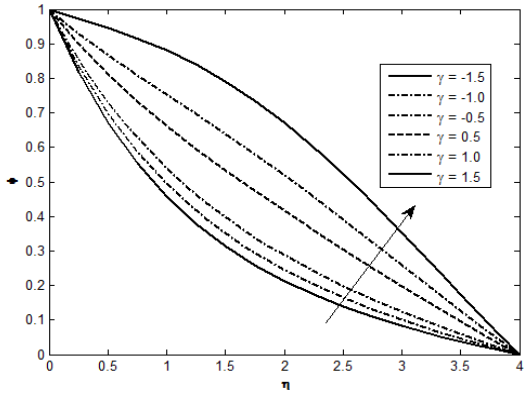

Fig14: Concentration profile for different values of γ

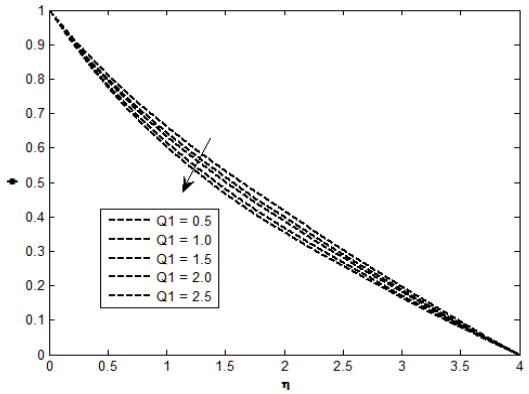

Fig15: Concentration profile for different values of Q_1

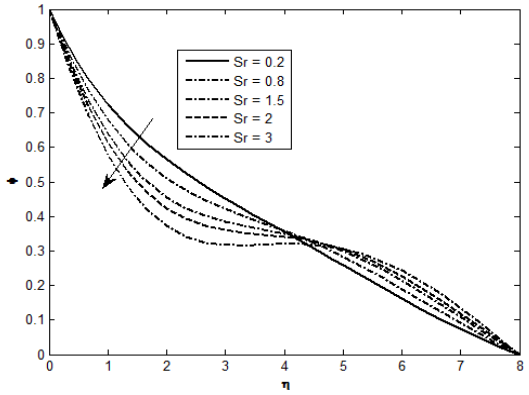

Fig16: Concentration profile for different values of Sr

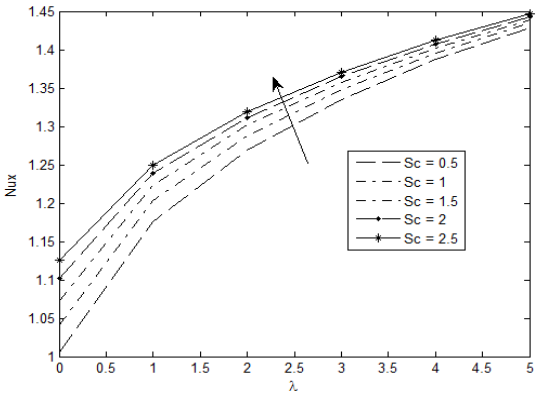

Fig17: Effect of λ on Nusselt Number for different values of Sc

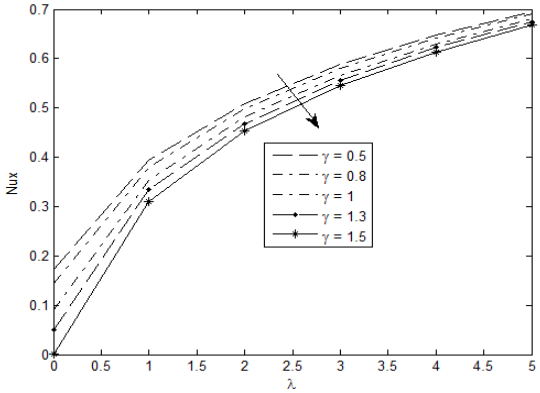

Fig18: Effect of λ on Nusselt Number for various values of γ

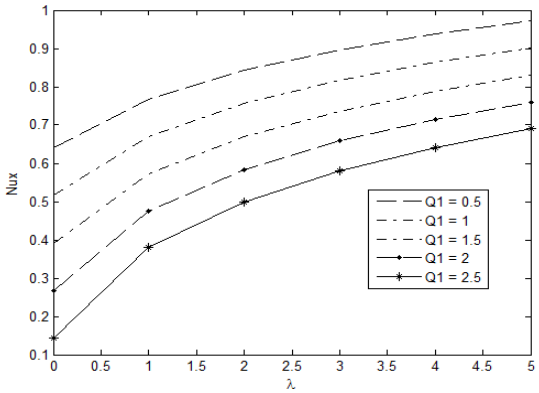

Fig19: Effect of λ on Nusselt Number for various values of Q_1

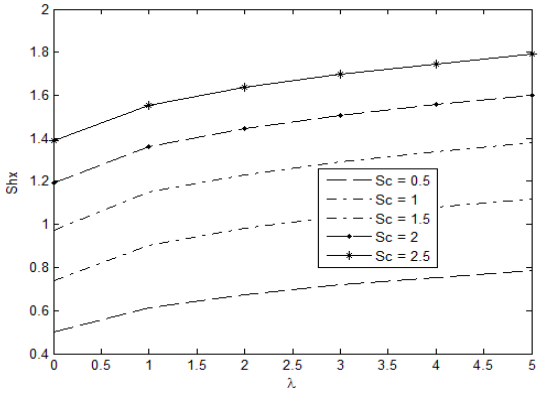

Fig20: Effect of λ on Sherwood number for various values of Sc

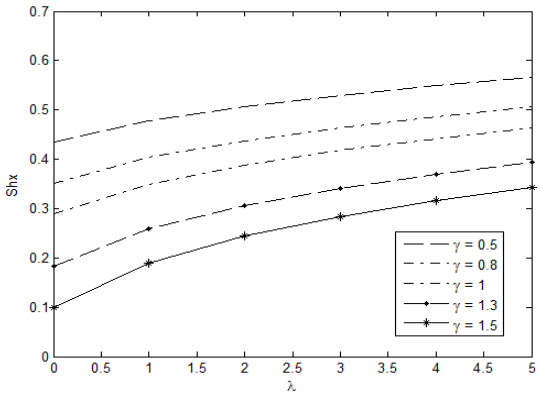

Fig21: Effect of λ on Sherwood number for various values of γ

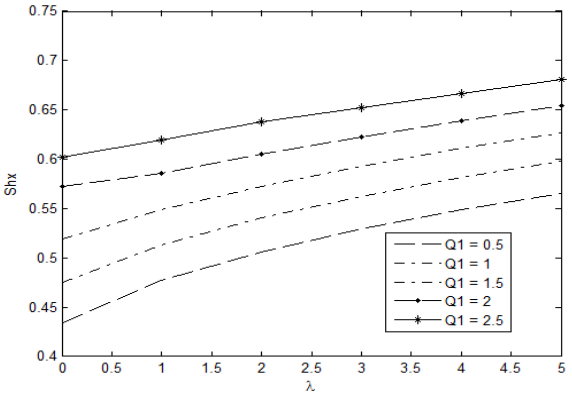

Fig22: Effect of λ on Sherwood number for various values of Q_1

increase in Sc is to decrease the concentration distribution. Physically, the increase of Sc means decrease in the molecular diffusivity which results in a decrease of concentration boundary layer. Hence the concentration is large for smaller values of Sc and lesser for higher values of Sc. Fig-(13) represent C with N. It is found that the concentration depreciates with N>0 when the buoyancy forces act in the same direction and for the forces acting in the opposite direction it enhances in the entire flow region. Fig-(14) represents C with chemical reaction parameter γ. It is found that the concentration distribution enhances in the degenerating chemical reaction case and depreciates in the generating chemical reaction case. Fig-(15) represents C with Q_1. The concentration depreciates with increase in Q_1 in the flow region. Fig-(16) represents C with Soret parameter Sr. It is found that an increase in Sr depreciates the concentration distribution in the region $0 \leq \eta \leq 4$ and enhances far away from the boundary.

The rate of heat transfer at $\eta = 0$ is shown in figures (17)-(19) for different values of Sc, γ and Q_1. The variation of Nu with Schmidt number Sc is shown in fig-(17). It is found that an increase in Sc results an enhancement in the rate of heat transfer at $\eta = 0$. The variation of Nu with chemical reaction parameter γ is shown in fig-(18). An increase in γ results in depreciation in the rate of heat transfer at $\eta = 0$ fixing the other parameter. We notice that the depreciation in Nu reduces as we move from the surface of the stretching sheet. From fig-(19) we notice that an increase in the radiation absorption parameter Q_1 is to decrease the rate of heat transfer at $\eta = 0$.

Figures (20)-(22) represents the Sherwood number (Sh) at the surface of stretching sheet at $\eta = 0$. Fig-(20) represents the Sherwood number Sh with Schmidt number Sc. It is found that lesser the molecular diffusivity larger the rate of mass transfer at the wall. The variation of Sh with chemical reaction parameter γ is exhibited in fig-(21). From this analysis we conclude that the rate of mass transfer at the wall $\eta = 0$ depreciates with increase in γ. Fig-(22) represents the Sherwood number Sh with radiation absorption Q_1. An increase in radiation absorption parameter Q_1 results in an enhancement in the rate of mass transfer at $\eta = 0$. As Q_1 increases the enhancement in Sh depreciates with higher values of Q_1.

ACKNOWLEDGEMENTS

One of the authors (B.Mallikarjuna) wished to thank the Dept. of Science & Technology, New Delhi, India for financial support to enable conducting this research work under Inspire fellowship. Authors thank the reviewers for their constructive suggestion and comments which have improved the quality of the paper considerably.

REFERENCES

[1]. Sakiadis BC. Boundary-layer behavior on continuous solid surfaces: 1.Boundary-layer equations for two-dimensional and axisymmetric flow. AICHE J. 7, 26-8, 1961.

[2]. Crane LJ. Flow past a stretching plane. J Appl Math Phys (ZAMP), 21, 645-7, 1970.

[3]. Muthucumaraswamy.R. and Ganesan.P. Effect of chemical reaction and injection on flow characteristics in an unsteady upward motion of an isothermal plate. J Appl Mech Tech Phys 42, 665-71, 2001.

[4]. Dulal Pal. Babulal Talukdar. Combined effects of Joule heating and chemical reaction on unsteady magnetohydrodynamic mixed convection of a viscous dissipating fluid over a vertical plate in porous medium with thermal radiation, Math Comput Modelling. 54, (11), 3016-3036, 2011.

[5]. Kalidas.D. Influence of thermophoresis and chemical reaction on MHD micropolar fluid flow with variable fluid properties. Int J Heat Mass Transfer. 55,(23), 7166-7174, 2012.

[6]. Krishnendu Battacharyya, Mass transfer on a continuous flat plate moving in parallel or reversely to a free stream in the presence of a chemical reaction, Int J Heat Mass Transfer 55,(13-14), 3482-3487, 2012

[7]. AY. Ghaly, MA. Seddeek, Chebyshev finite difference method for the effect of chemical reaction , heat and mass transfer on laminar flow along semi-infinite horizontal plate with temperature dependent viscosity, Choas Solitons Fractals 19 (5), 61-70, 2004.

[8]. JA. Rao, S. Shivaiah, Chemical reaction effect on unsteady MHD flow past semi-infinite vertical porous plate with viscous dissipation, Appl Math Mech 32, (8), 1065-1078, 2011.

[9].Chapman S. and Cowling TG. The mathematical theory of non-uniform gases. Cambridge. UK: Cambridge Univ. Press: 1952.

[10] Hirshfelder JO. Curtis CF. Bird RB. Molecular theory of gases and liquids. New York: Weley: 1954.

[11] Ali ME. The effect of variable viscosity on mixed convection heat transfer along a vertical moving surface. Int J Thermal Sci 2006;45:60-9.

[12] Dulal Pal. Hiranmoy Mondal. MHD non-Darcy mixed convective diffusion of species over a stretching sheet embedded in a porous medium with non-uniform heat source/sink, ariable viscosity and Soret effect. Commun Nonlinear Sci Numer Simulat. 17, 672-684, 2012.

[13] Ibrahim.F.S., Elaiw.A.M. and Bakr.A.A. Effect of the chemical reaction and radiation absorption on the unsteady MHD free convection flow past a semi infinite vertical permeable moving plate with heat source and suction. Communication in Nonlinear Science and Numerical Simulation. 13, 1056-1066, 2008.

[14] Lai EC. Kulacki. FA. Effects of variable viscosity on connective heat transfer along a vertical surface in a saturated porous medium. Int J Heat Mass Transfer. 33, 1028-31, 990.

[15] Pal D. Mondal H. Effect of variable viscosity on MHD non-Darcy mixed convective heat transfer over a stretching sheet embedded in a porous medium with non-uniform heat source/sink. Commun Nonlinear Sci Numer Simulat. 15, 1553-64, 2006.

[16] Seddeek MA, Almushigeh AA. Effects of radiation and variable viscosity on MHD free convective flow and mass transfer over a stretching sheet with chemical reaction. Appl. Math. 5(1), 181-97, 2010.

[17] Abo-Eldahab Emad M, El Aziz Mohamed A. Blowing/suction effect on hydromagnetic heat transfer by mixed convection from an inclined continuously stretching surface with internal heat generation/absorption. Int J Thermal Sci. 43, 709-19, 2004.

[18] Tsai R. Huang KH. Huang JS. Flow and heat transfer over an unsteady stretching surface with non-uniform heat source. Int Commun Heat Mass Transfer. 35, 1340-3, 2008.

[19] Bathe. K.J. Finite Element Procedures. Prentice-Hall, New Jersey. 1996.

[20] Reddy. JN. An introduction to the Finite Element Method, Second ed., McGraw-Hill, New York. 1985.

[21] Dulal Pal. Hiranmoy mondal. MHD non-Darcy mixed convective diffusion species over a stretching sheet embedded in a porous medium with non-uniform heat source/sink, variable viscosity and Soret effect. Commun Nonlinear Sci Number Simulat. 17, 672-684, 2012.

[22] Ishak. A. Nazar. R. Pop. I. Hydromagnetic flow and heat transfer adjacent to a stretching vertical sheet. Heat Mass Transfer. 44. 921-7, 2008.

[23] Grubka. LG. Bobba. KM. Heat transfer characteristics of a continuous stretching surface with variable temperature. ASME J Heat Transfer. 107, 248-50, 1985.

[24] Abel. M. Siddheshwar. PG. Nandeppanavar. MM. Heat transfer in a viscoelastic boundary layer flow over a stretching sheet with viscous dissipation and non-uniform heat source. Int J Heat Mass Transfer. 50, 960-6, 2007.

Source of support: Nil, Conflict of interest: None Declared

